CuMoRu ternary nanorods: synergy effect of metal elements enables efficient electrochemical CO_2 reduction towards selective ethanol production

Dong Xiang*[a, b, c], Huanzong Liao[a], Ziyi Gui[c], Dezhong Hu[c], Kunzhen Li,[c] Kanghua Miao,[c] Aidar Kuchkaev[d], Dmitry G. Yakhvarov[d], Xiongwu Kang*[c], Xiufang Wang*[a]

a School of Pharmacy, Guangdong Pharmaceutical University, Guangzhou 510006, Guangdong, China

b College of Chemistry, Bohai University, Jinzhou, 121013, China

c New Energy Research Institute, School of Environment and Energy, South China University of Technology, 382 East Waihuan Road, Higher Education Mega Center, Guangzhou 510006, China

d Arbuzov Institute of Organic and Physical Chemistry, FRC Kazan Scientific Center of RAS, Arbuzov Street 8, Kazan 420088, Russian Federation

*Email: xiangdong@bhu.edu.cn (D. Xiang), esxkang@scut.edu.cn (X. Kang), xiufang Wang: x_f_wang@163.com

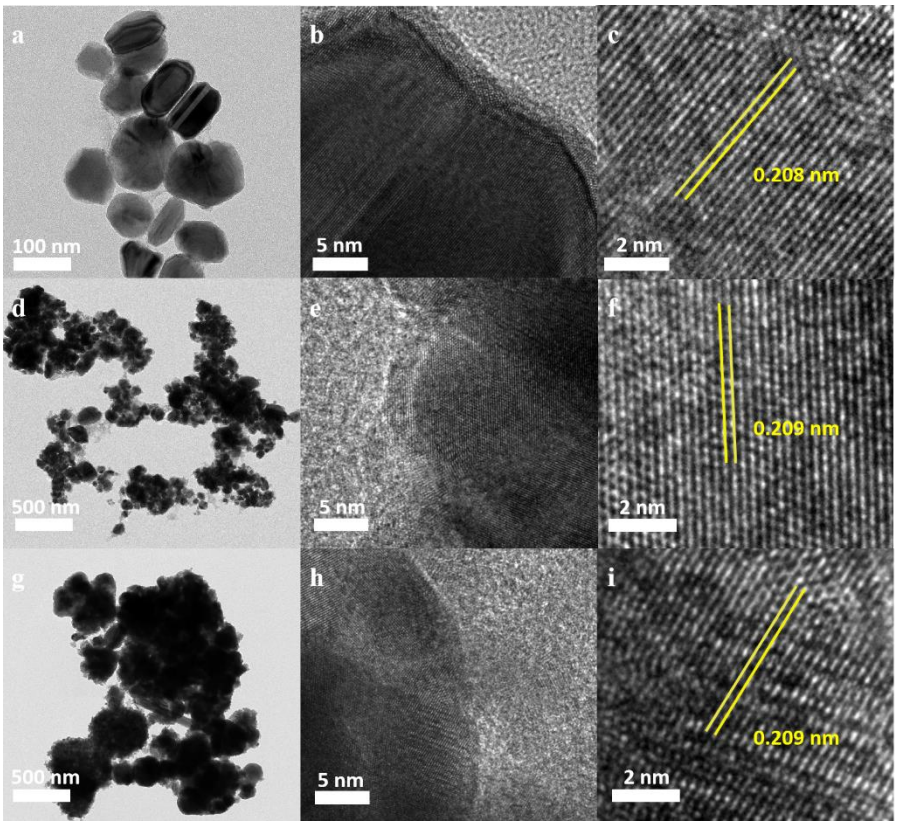

Figure S1. TEM and HRTEM images of (a-c) Cu, (d-e) CuRu and (g-i) CuMo.

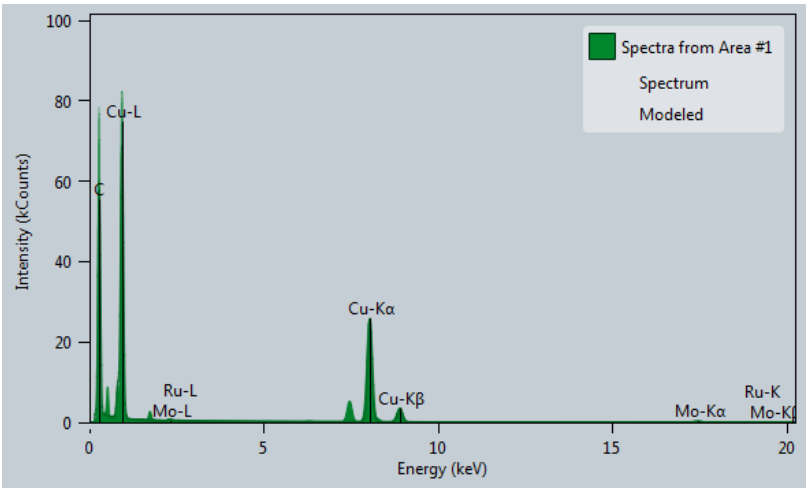

Figure S2. EDS spectrum of CuMoRu obtained in TEM characterization.

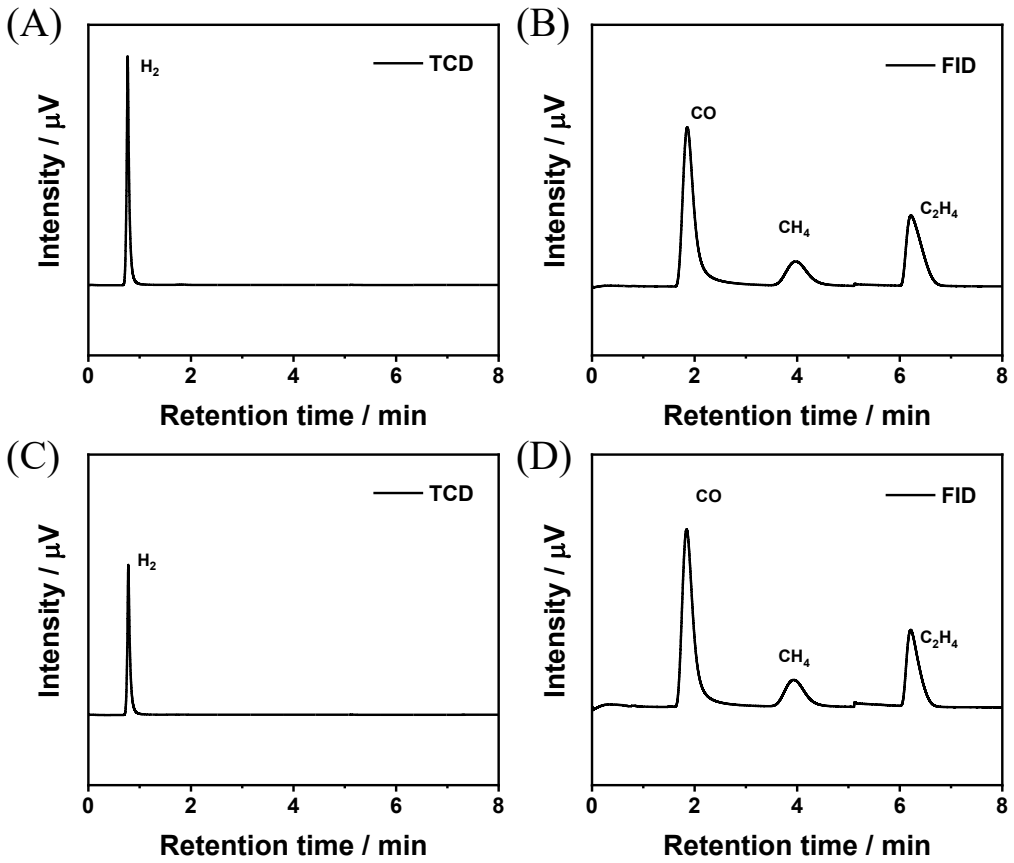

Figure S3. Gas chromatography plots for determining gas products of eCO_2RR on (A-B) Cu and (C-D) CuMo at −1.1 V vs. RHE in 1.0 M KOH aqueous electrolyte.

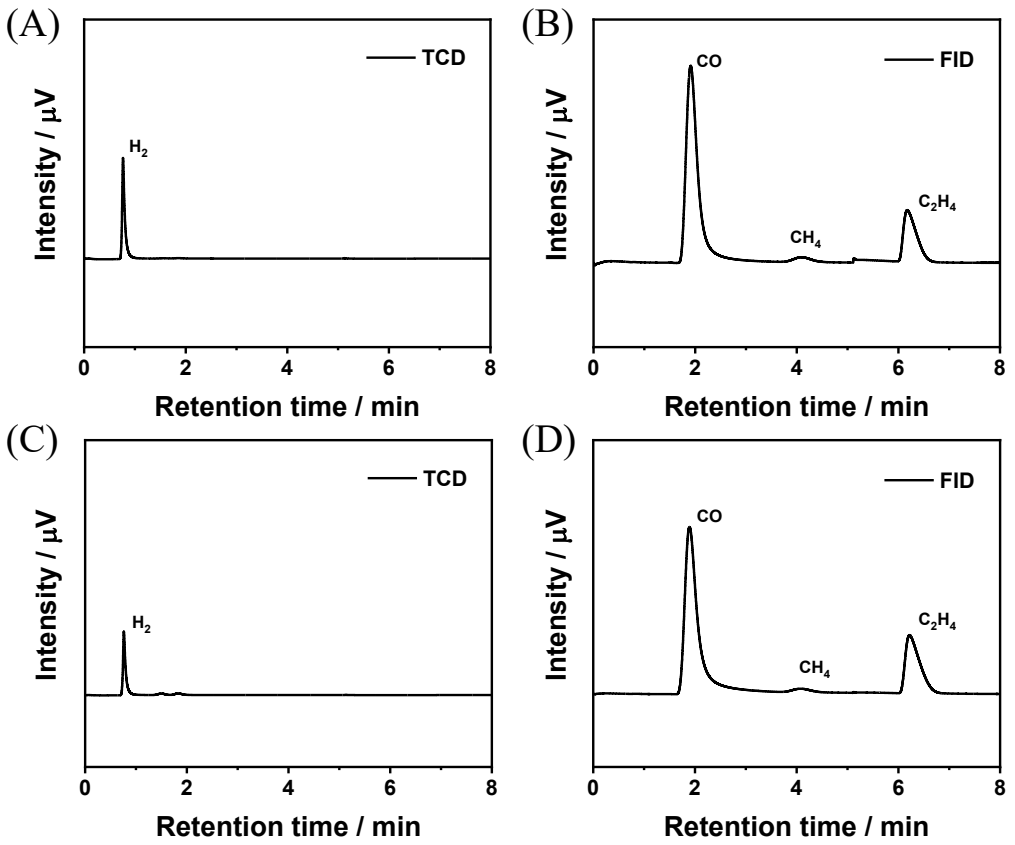

Figure S4. Gas chromatography plots for determining gas products of eCO_2RR on (A-B) CuRu and (C-D) CuMoRu at −1.1 V vs. RHE in 1.0 M KOH electrolyte.

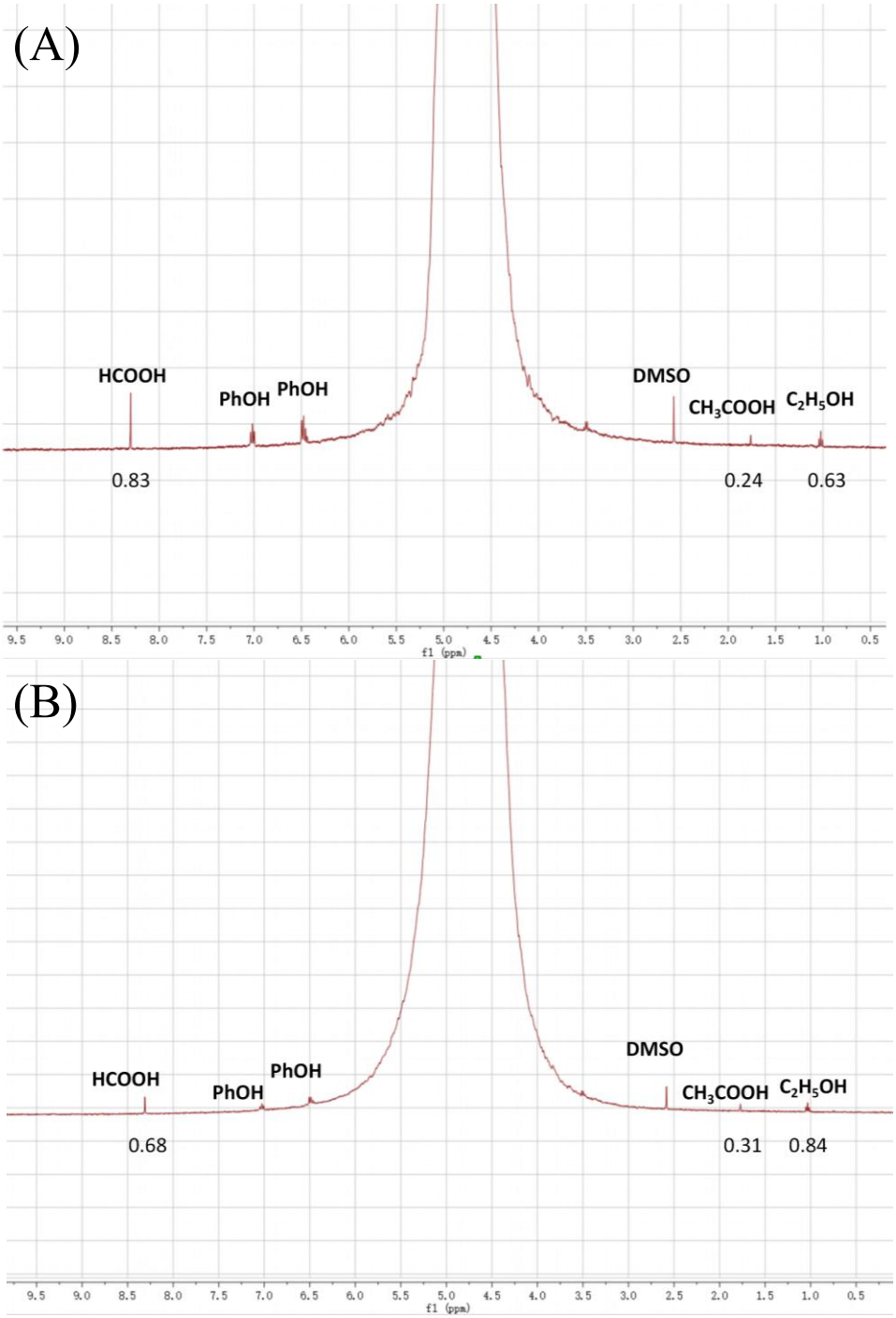

Figure S5. ^{1}H-NMR spectrum and the corresponding the integral values for liquid products of (A) Cu and (B) CuMo catalysts at −1.1 V vs. RHE in 1.0 M KOH electrolyte, with dimethyl sulfoxide (DMSO) and phenol (PhOH) as an internal standard.

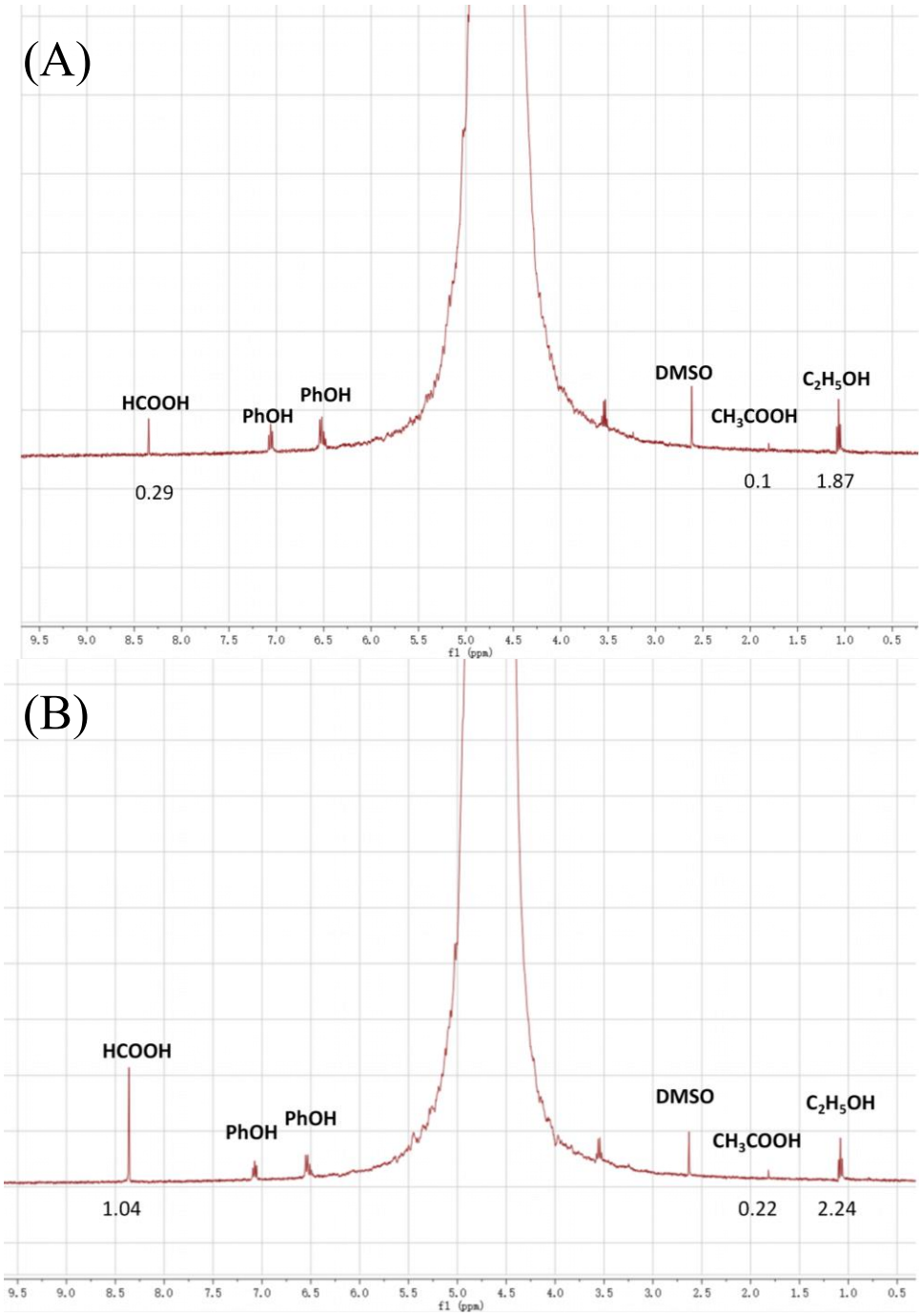

Figure S6. ^{1}H-NMR spectrum and the corresponding the integral values for liquid products of (A) CuRu and (B) CuMoRu catalysts at −1.1 V vs. RHE in 1.0 M KOH electrolyte, with dimethyl sulfoxide (DMSO) and phenol (PhOH) as an internal standard.

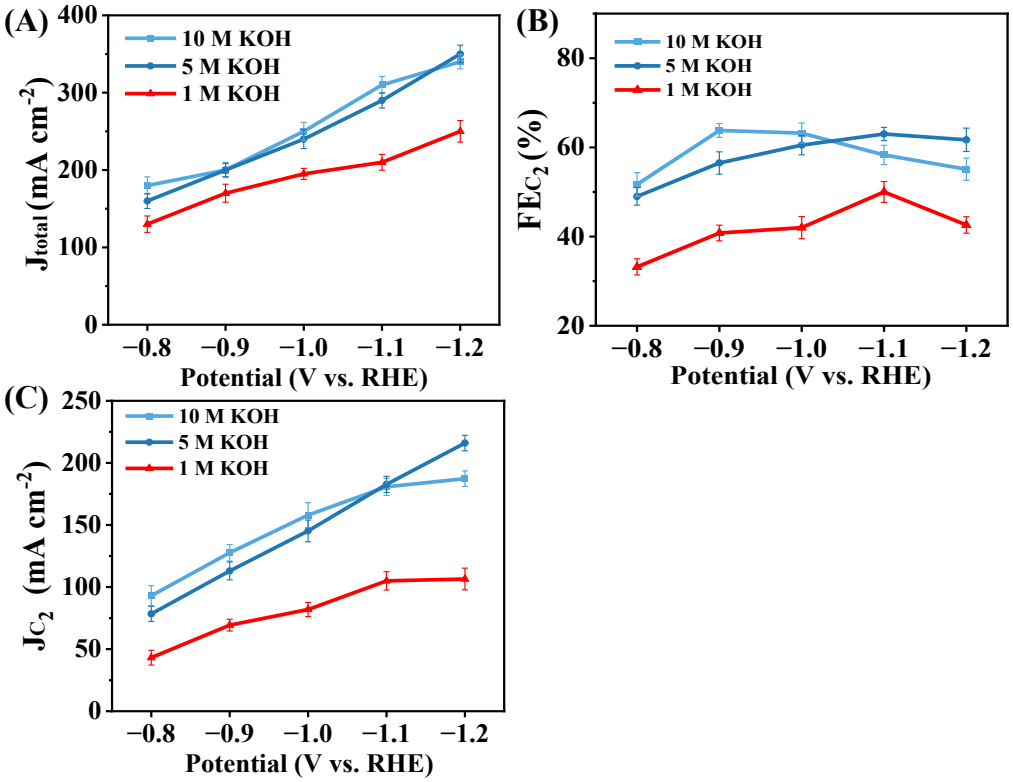

Figure S7. (A) Total current density, FE of C_2 products and (C) partial current density of eCO_2RR on CuMoRu in 1.0 M, 5.0 M, and 10.0 M KOH electrolyte.

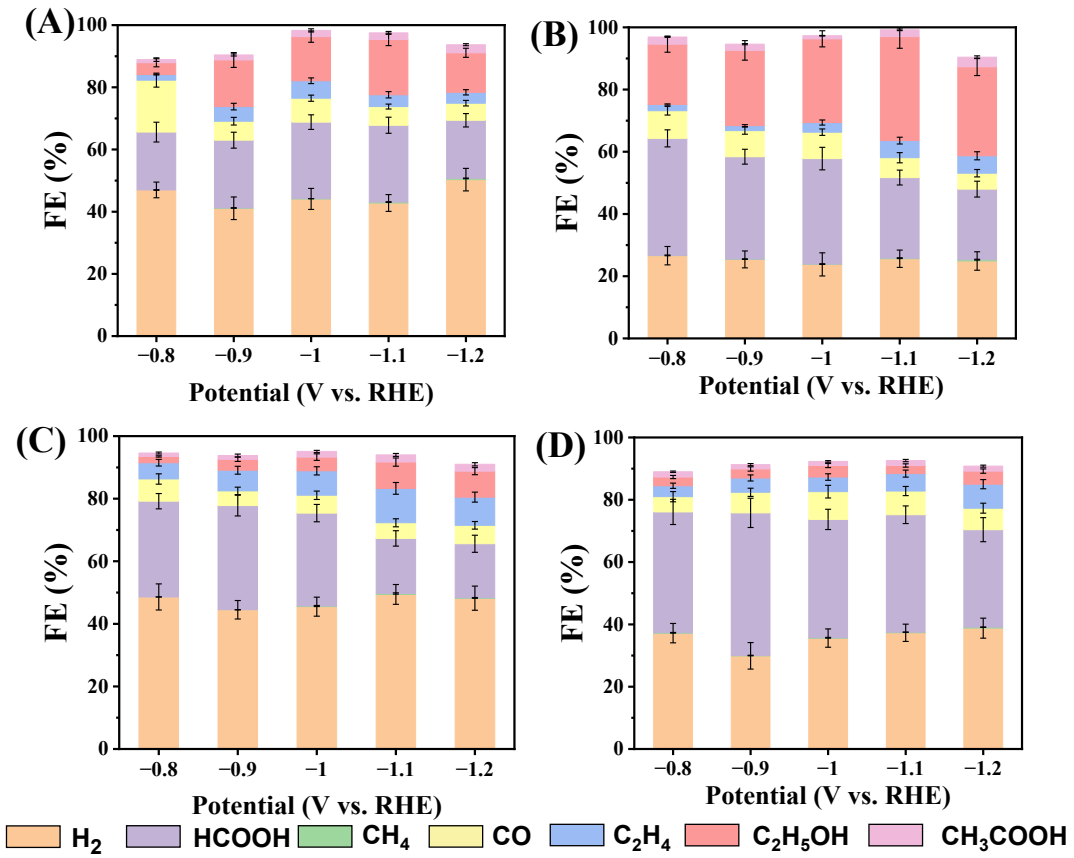

Figure S8. FE of eCO_2RR products on (A) CuMoRu-5, (B) CuMoRu-3, (C) CuMoRu-2 and (D) CuMoRu-1 in 1.0 M KOH electrolyte.

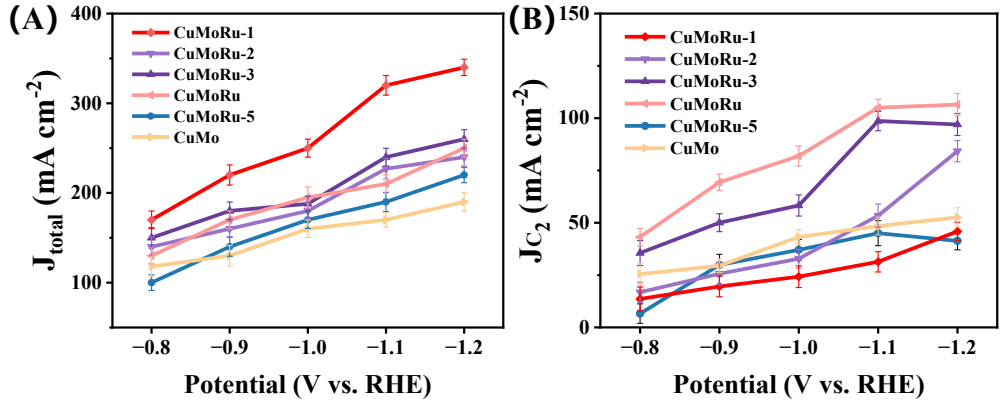

Figure S9. (a) Total current density and (b) partial current density of C_2 products of CuMo, CuMoRu and CuMoRu-X (X=1, 2, 3, 5).

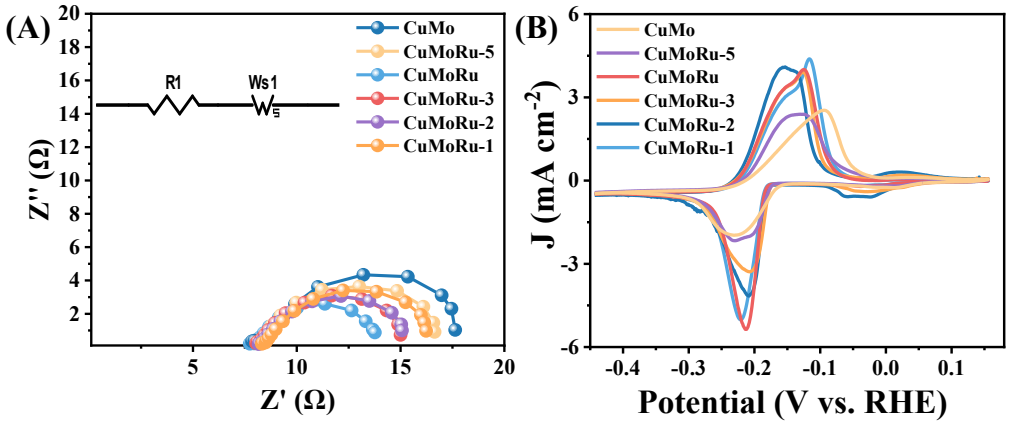

Figure S10. (a) Nyquist plots of EIS spectra of eCO$_2$RR on CuMo, CuMoRu and CuMoRu-X (X=1, 2, 3, 5). (b) Cyclic voltammetry of Pb underpotential deposition of CuMo and CuMoRu-X samples.

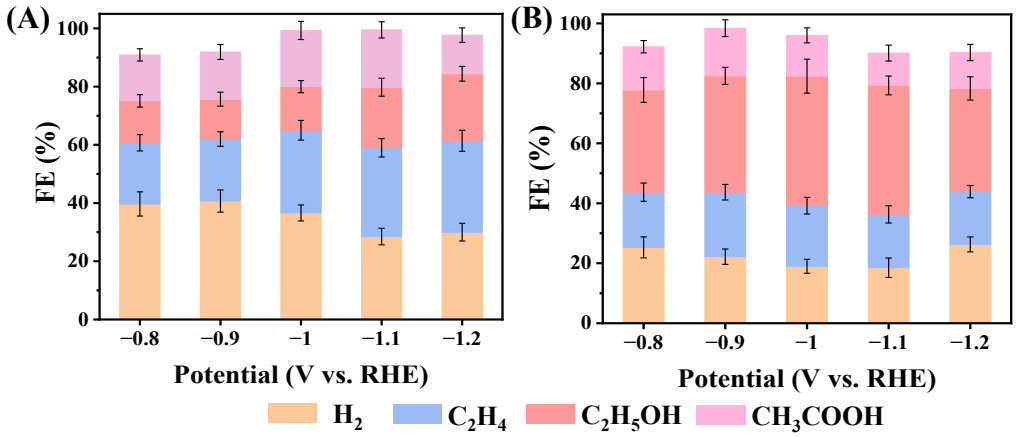

Figure S11. The FEs of CuMo and CuMoRu in 1.0 M KOH for CORR in flow cell.

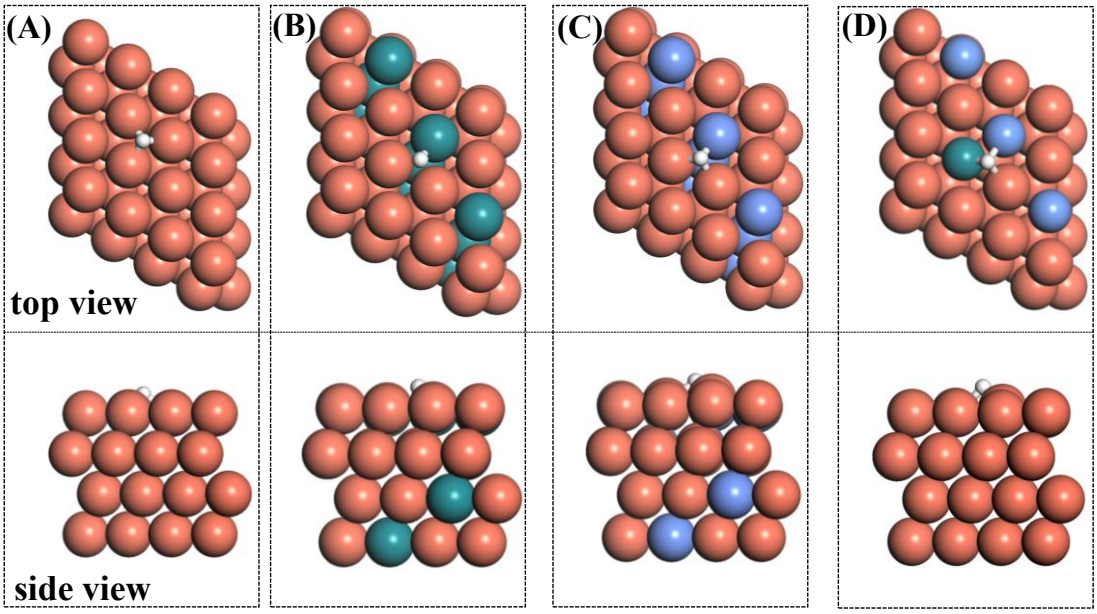

Figure S12. The configurations for *H on (a) Cu (111), (b) CuRu (111), (c) CuMo (111) and (d) CuMoRu (111) (top view and side view). The brick red, green, blue, grey, red and white balls represent Cu, Ru, Mo, C, O and H, respectively.

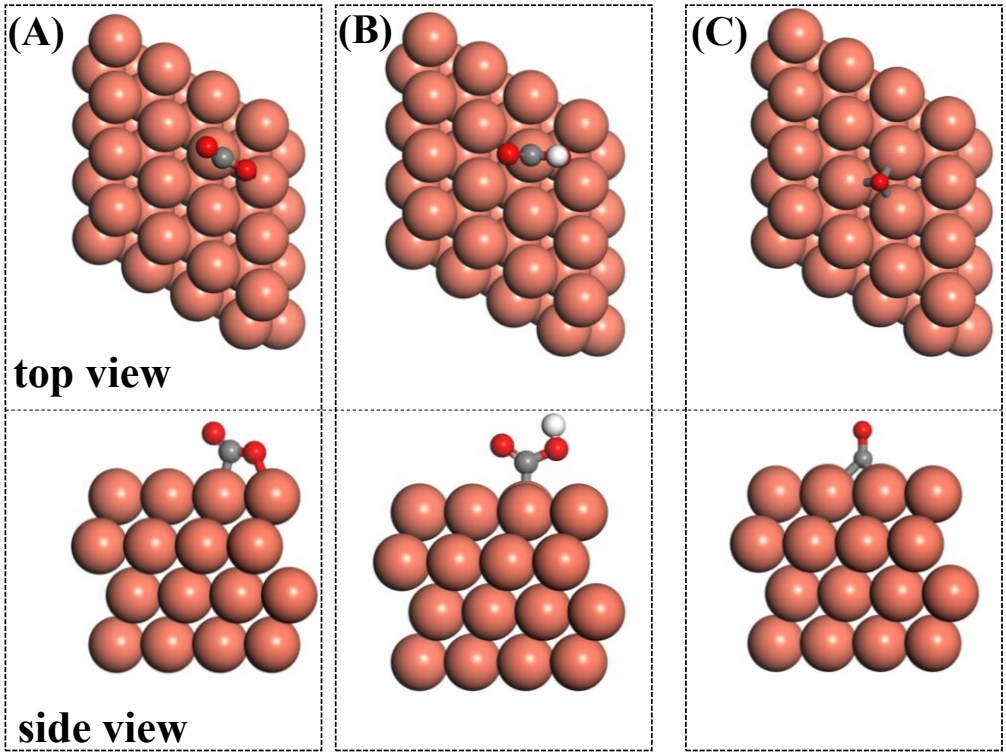

Figure S13. The configurations for (a) *CO_2, (b) *COOH and (c) *CO on Cu (111) (top row: top view; bottom row: side view). The grey, red and white balls represent C, O and H, respectively.

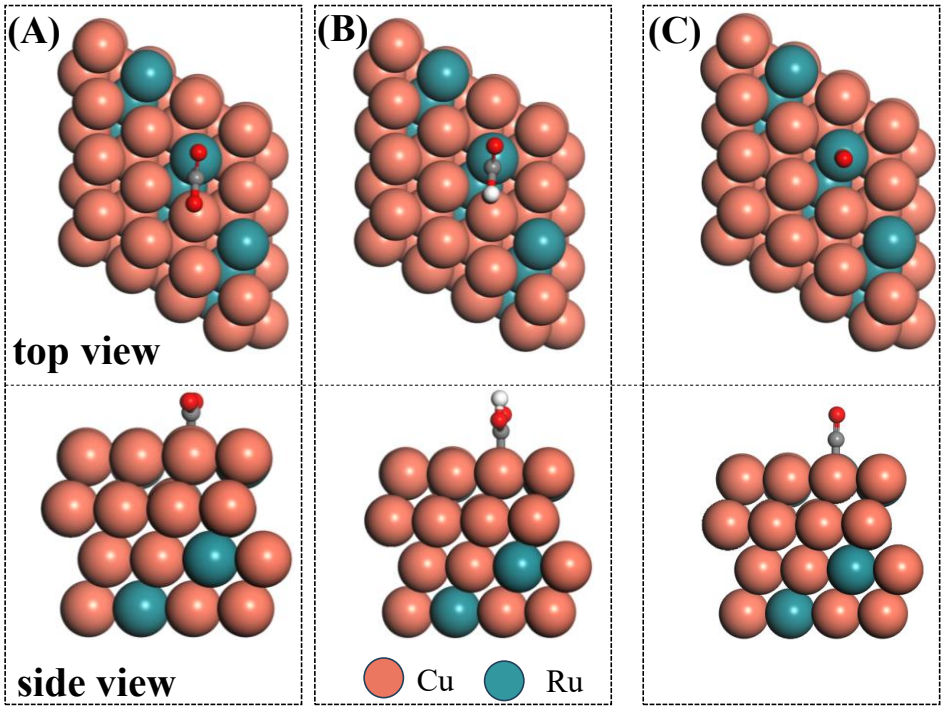

Figure S14. The configurations for (A) *CO_2 (B) *COOH and (C) *CO on CuRu (111) (top row: top view; bottom row: side view). The grey, red and white balls represent C, O and H, respectively.

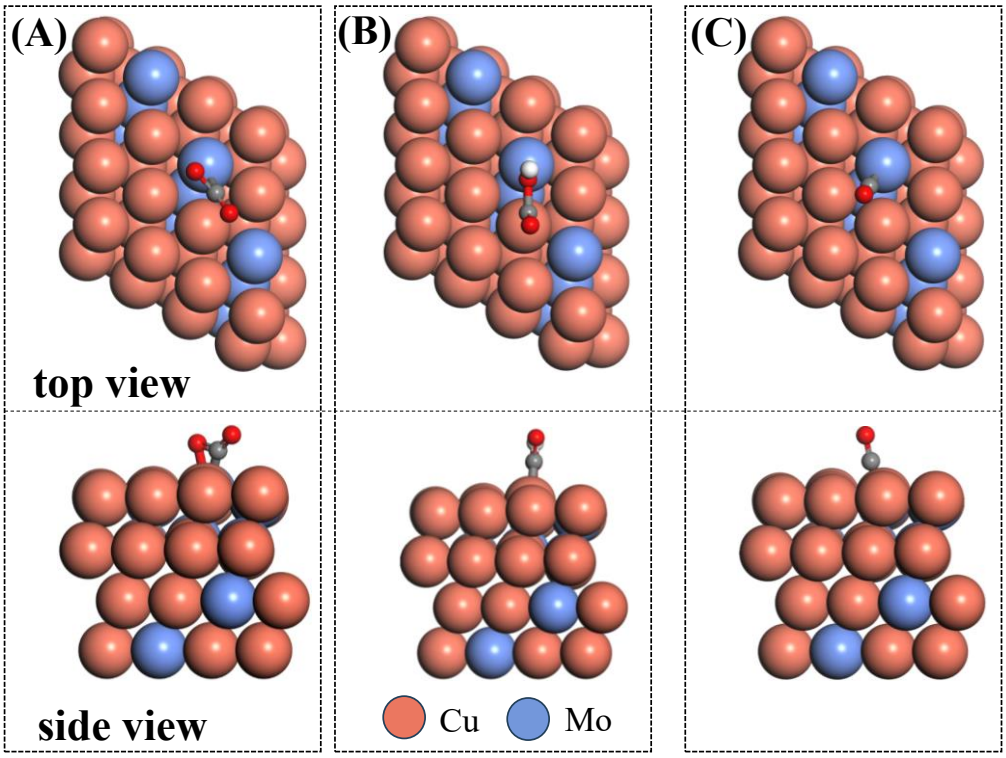

Figure S15. The configurations for (a) *CO_2, (b) *COOH and (c) *CO on CuMo (111) (top row: top view; bottom row: side view). The grey, red and white balls represent C, O and H, respectively.

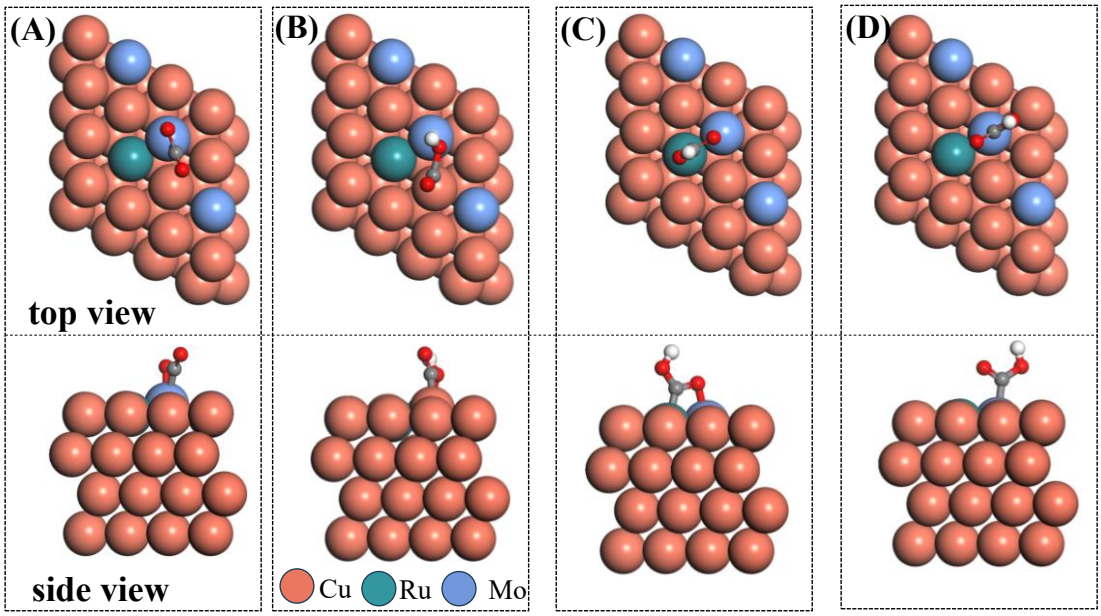

Figure S16. The configurations for (a) *CO_2, and *COOH on (b) Mo site (c) Cu site and (d) Ru site of CuMoRu (111) (top row: top view; bottom row: side view). The grey, red and white balls represent Cu, Ru, Mo, C, O and H, respectively.

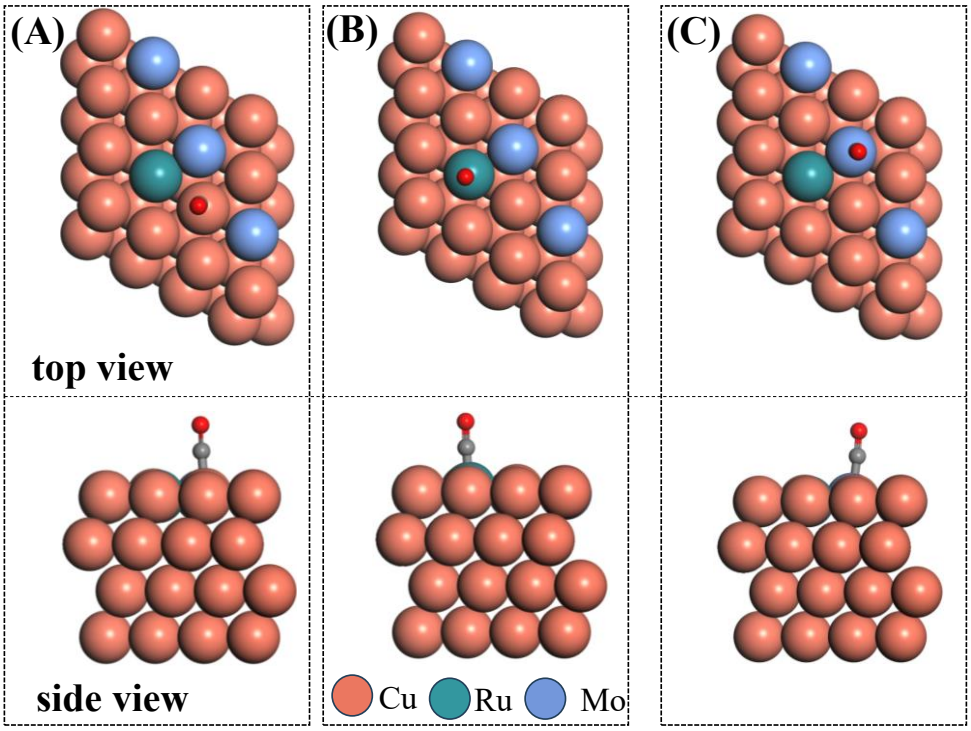

Figure S17. (a) The configurations of *CO on (a) Cu site, (b) Mo site and (c) Ru site on CuMoRu (111) (top row: top view; bottom row: side view). The brick red, green, blue, grey, red and white balls represent Cu, Ru, Mo, C, O and H, respectively.

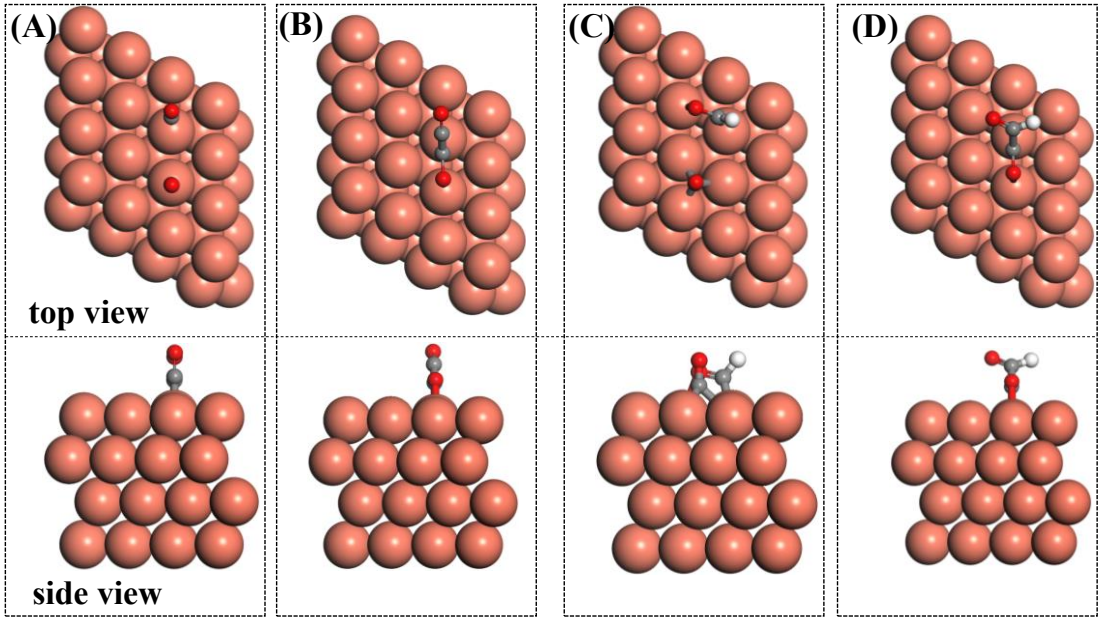

Figure S18. The configurations for dimerization of (A) 2*CO and (B) *OCCO on Cu (111). The configurations for dimerization of (C) *CO and *CHO (D) COCHO on Cu (111) (top row: top view; bottom row: side view). The brick red, grey, red and white balls represent Cu, C, O and H, respectively.

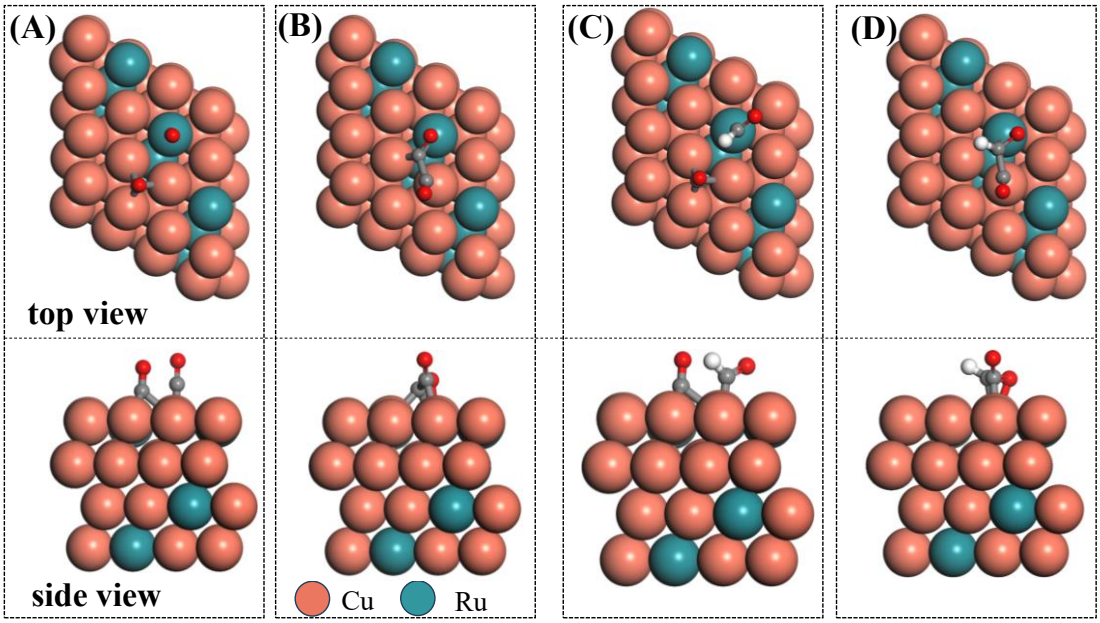

Figure S19. The configurations for dimerization of (A) 2*CO and (B) *OCCO on Cu Ru (111). The configurations for dimerization of (C) *CO and *CHO and (D) COCHO on CuRu (111) (top view and side view). The brick red, green, grey, red and white balls represent Cu, Ru, C, O and H, respectively.

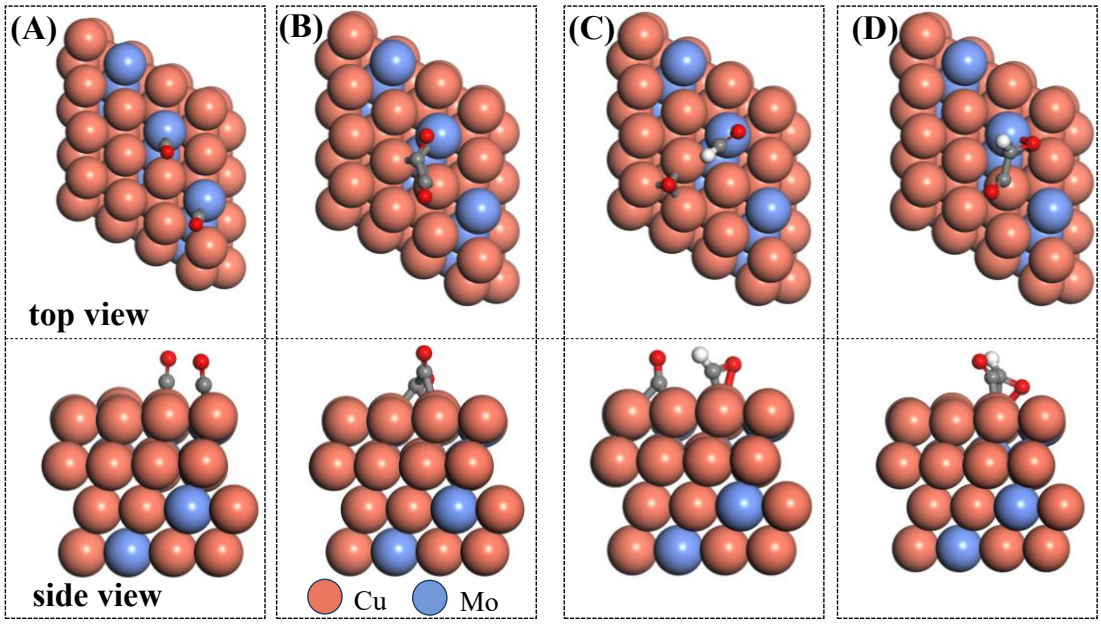

Figure S20. The configurations for dimerization of (A) 2*CO and (B) *OCCO on CuMo (111). The configurations for dimerization of (C) *CO and *CHO and (D) COCHO on CuMo (111) (top view and side view). The brick red, blue, grey, red and white balls represent Cu, Mo, C, O and H, respectively.

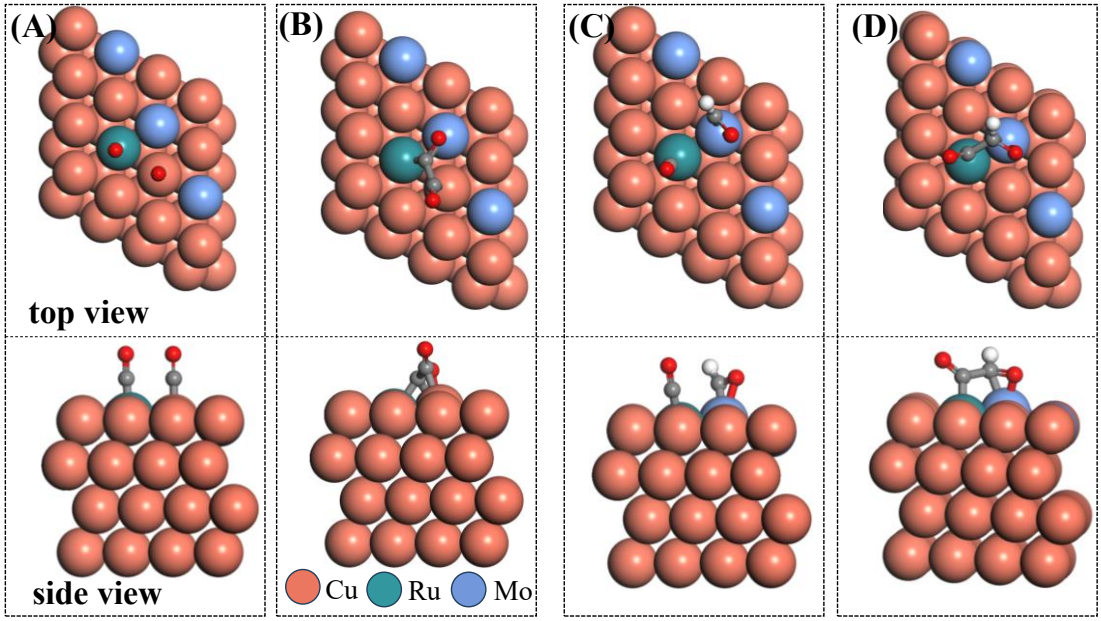

Figure S21. The configurations for dimerization of 2*CO and *OCCO on (a-b) MoRu-Cu (111). The configurations for dimerization of *CO and *CHO (c-d) and (D) COCHO MoRu-Cu (111) (top view and side view). The brick red, green, blue, grey, red and white balls represent Cu, Ru, Mo, C, O and H, respectively.

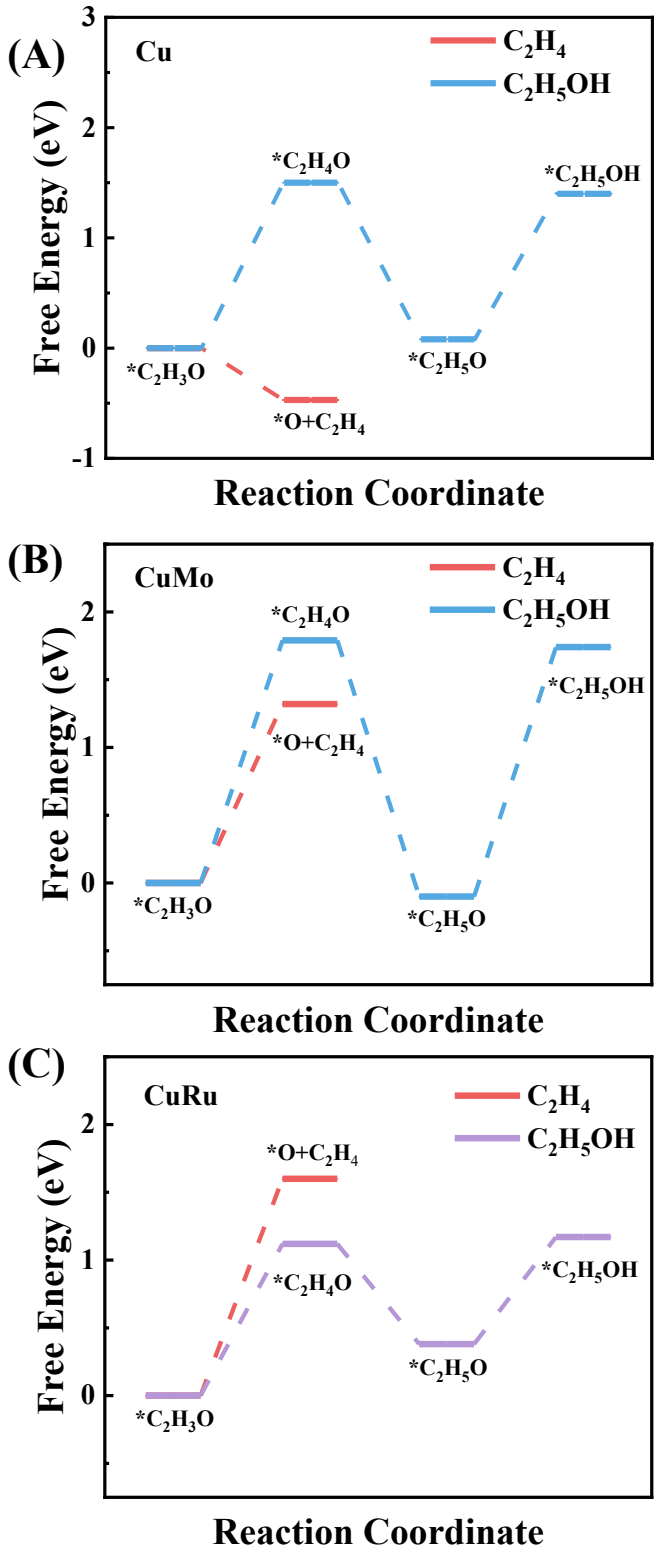

Figure S22. Gibbs free energy diagram to C_2H_4 (red) and C_2H_5OH (blue) on (A) CuMo (111) and (B) CuRu (111).

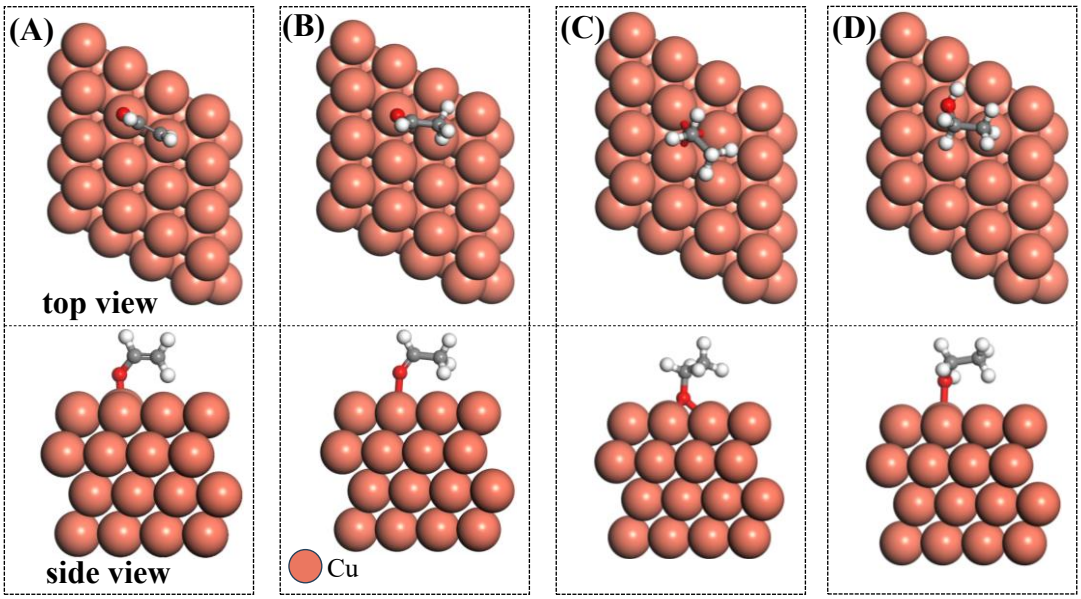

Figure S23. The configurations for (A) *CH_2CHO, (B) *CH_3CHO, (C) *CH_3CH_2O and (d) *CH_3CH_2OH during eCO_2RR to C_2H_5OH on Cu (111) (top row: top view; bottom row: side view). The balls represent Cu, C, O and H, respectively.

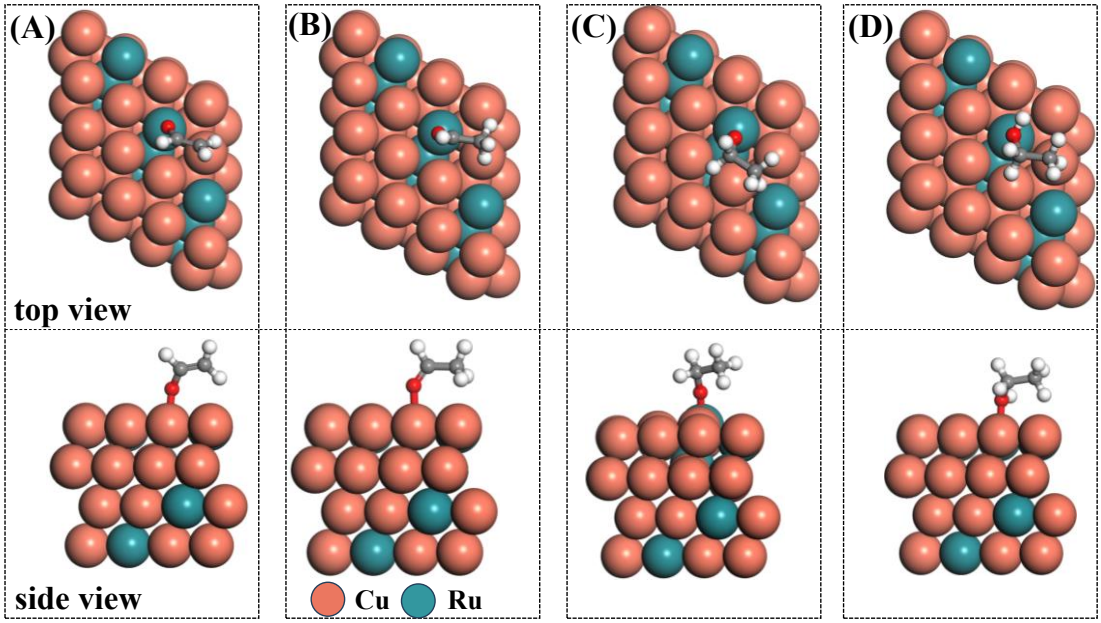

Figure S24. The configurations for (A) *CH_2CHO, (B) *CH_3CHO, (C) *CH_3CH_2O and (d) *CH_3CH_2OH during eCO_2RR to C_2H_5OH on CuRu (111) (Top row: top view; Bottom row: side view). The grey, red and white balls represent C, O and H, respectively.

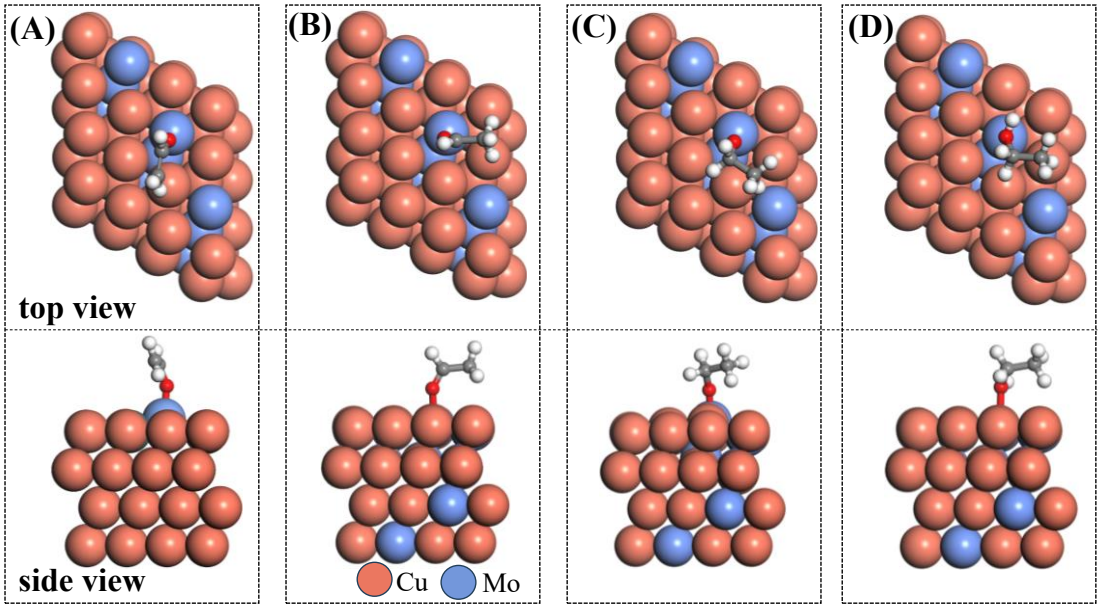

Figure S25. The configurations for (A) *CH_2CHO, (B) *CH_3CHO, (C) *CH_3CH_2O and (D) *CH_3CH_2OH during eCO_2RR to C_2H_5OH on CuMo (111) (Top row: top view; Bottom row: side view). The grey, red and white balls represent C, O and H, respectively.

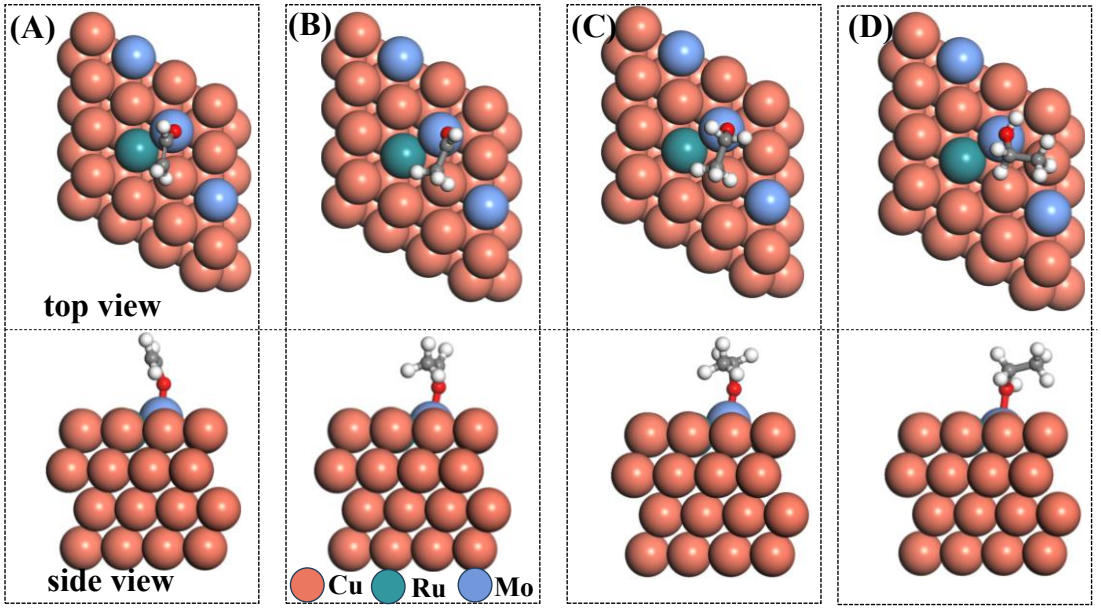

Figure S26. The configurations for (A) *CH_2CHO, (B) *CH_3CHO, (C) *CH_3CH_2O and (D) *CH_3CH_2OH during eCO_2RR to C_2H_5OH on CuMoRu (111) (Top row: top view; Bottom row: side view). The brick grey, red and white balls represent, C, O and H, respectively.

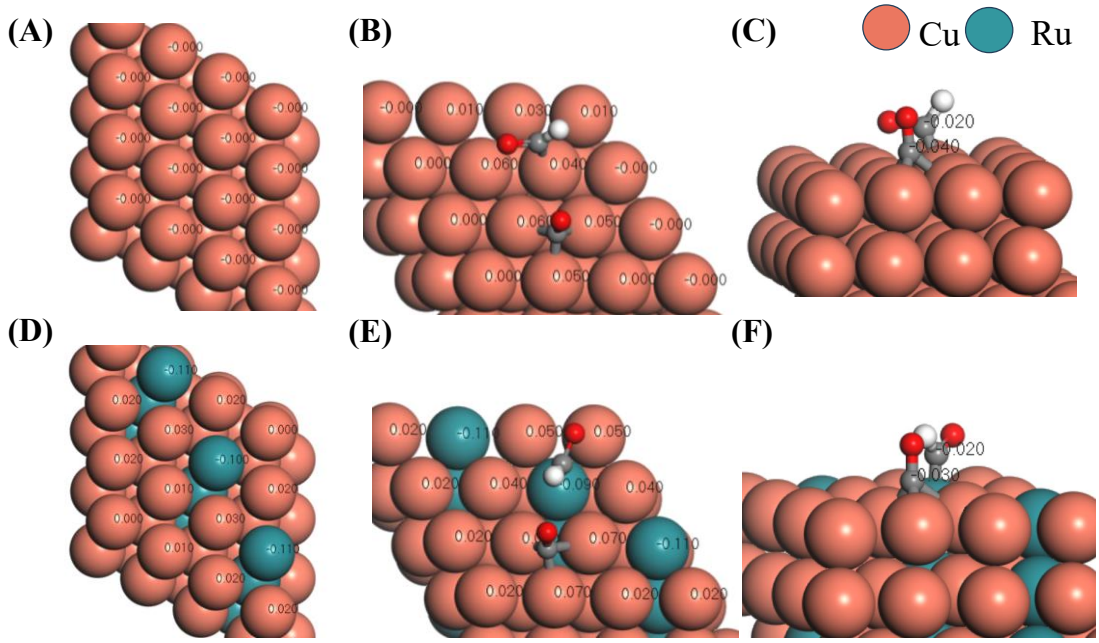

Figure S27. Bader charge of (A) Cu (111); (B) top view of Cu (111) with adsorbed CO and CHO; (C) side view of Cu (111) with CO and CHO; Bader charge of (D) CuRu (111), (E) top view of CuRu (111) with adsorbed CO and CHO; (F) side view of CuRu (111) with CO and CHO.

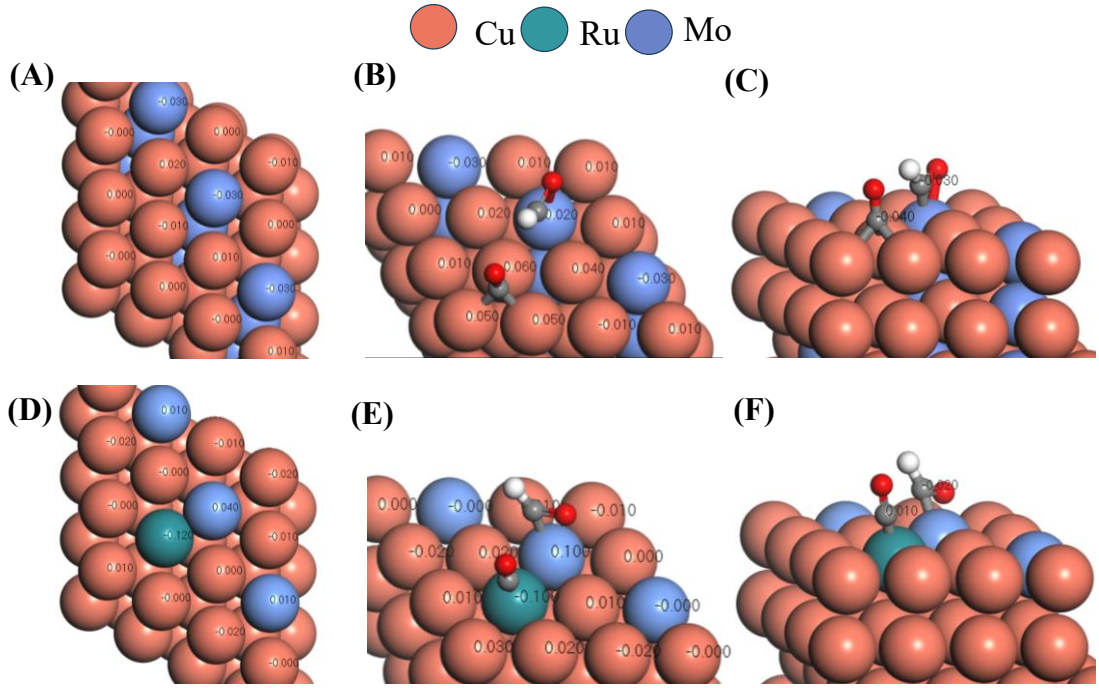

Figure S28. Bader charge of (A) CuMo (111); (B) top view of CuMo (111) with adsorbed CO and CHO; (C) side view of CuMo (111) with CO and CHO; Bader charge of (D) CuMoRu (111), (E) top view of CuMoRu (111) with adsorbed CO and CHO; (F) side view of CuMoRu (111) with CO and CHO.

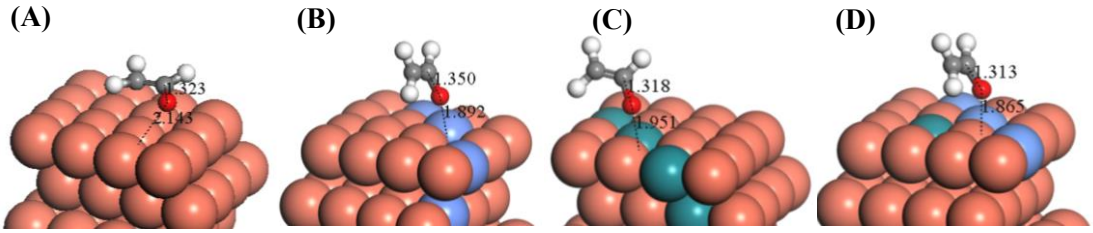

Figure S29. Schematic illustration of key intermediate *C_2H_3O on (a) Cu (111), (b) CuMo (111), CuRu (111) and CuMoRu (111). The grey, red and white balls represent C, O and H, respectively.

Table S1. Atomic Fraction (%) of metal elements in CuMoRu determined by EDS spectrum and atomic ICP-AES.

Element	**Atomic Fraction (%) by EDS**	**Atomic Fraction (%) by ICP-AES**
Cu	95.61	94.11
Mo	3.99	4.86
Ru	0.40	1.03

Table S2. Atomic percentage of metal components in CuMo, CuMoRu and CuMoRu-X (X=1, 2, 3 and 5) samples determined by XPS high-resolution spectra.

%	**Cu**	**Mo**	**Ru**
CuMo	74.9	25.1	-
CuMoRu-5	53.3	33.8	12.9
CuMoRu	59.4	28.7	11.9
CuMoRu-3	61.7	14.4	23.8
CuMoRu-2	50.4	18.4	31.3
CuMoRu-1	54.4	12.8	32.7

Table S3. Comparison of FE and partial current density for ethanol production in eCO_2RR of CuMoRu in this study with previous reported binary alloy and any other catalysts.

Catalysts	FE (%)	J (mA cm^{-2})	electrolyte	stability	Reference
CuMoRu	**51.8**	**182.7**	**KOH**	**over 10 h**	**This work**
P-Cu	18.0	49.5	KOH	12 h	1
PAMV-Cu	57.3	51.4	$CsHCO_3$	20 h	2
Cu_2S-Cu-V	25.0	100.0	KOH	-	3
Pb-Cu	50	131	KOH	200 h	4
$Cu_2O@Cu_2S$	43.9	70.2	$KHCO_3$	24 h	5
Ag_1Cu NW	56.3	97.3	KOH	7 h	6
F-Cu_2O	55.2	166	KOH	60 h	7
$CuAl_2O_4$/CuO	41.0	82.0	KOH	150 h	8
$Cu+COP_{CO+OH}$	54.2	121.3	$KHCO_3$	100 h	9

Table S4. The EIS fitted equivalent circuit parameters from EIS and ECSA (cm^{-2}) of CuMo, CuMoRu and CuMoRu-X (X=1, 2, 3 and 5) samples.

Samples	R_{ct} / Ω	*W-R* /Ω·cm²·s$^{-1/2}$	*W-T* / mΩ·cm²·s$^{-1/2}$	*W-P* / Ω·cm²·s$^{-1/2}$	ECSA / cm^{-2}
CuMo	7.71	10.52	2.4	0.50	0.92
CuMoRu-5	7.80	8.90	5.7	0.51	0.93
CuMoRu	7.36	6.16	5.5	0.51	1.12
CuMoRu-3	7.75	7.49	3.9	0.49	1.12
CuMoRu-2	7.77	7.99	7.5	0.46	1.13
CuMoRu-1	8.06	8.43	7.6	0.49	1.13

R_{ct}: Interfacial charge transfer resistance. W-R represents the diffusion coefficient and measure of how quickly the species can diffuse to the electrode surface. W-T is defined as L^2/D, where L is the thickness of the diffusion layer and D is the diffusion coefficient. W-P is a dimensionless parameter, which is typically 0.5 for Warburg diffusion, indicating the power-law relationship between impedance and frequency. It reflects the characteristic 45° phase angle observed in the Nyquist plot for Warburg impedance. The deviation from 0.5 might be accounted for the roughness or porosity of the electrode layers.

Reference

1. X. Kong, C. Wang, H. Zheng, Z. Geng, J. Bao and J. Zeng, *Science China Chemistry*, 2021, 64, 1096-1102.
2. W. Yuan, Z. Zhao, G. Tao, L. He, Y. Wang, Q. Qian, J. Zhang, L. Jing, J. Ma, Y. Yuan, B. Guan, X. Sun and B. Han, *Journal of the American Chemical Society*, 2026, DOI: 10.1021/jacs.5c20004.
3. T.-T. Zhuang, Z.-Q. Liang, A. Seifitokaldani, Y. Li, P. De Luna, T. Burdyny, F. Che, F. Meng, Y. Min, R. Quintero-Bermudez, C. T. Dinh, Y. Pang, M. Zhong, B. Zhang, J. Li, P.-N. Chen, X.-L. Zheng, H. Liang, W.-N. Ge, B.-J. Ye, D. Sinton, S.-H. Yu and E. H. Sargent, *Nature Catalysis*, 2018, 1, 421-428.
4. P. Liu, N. Sun, J. Su, Y. Wang, Z. Peng, S. Chen, P. Papangelakis, A. Ozden, R. K. Miao, X. Wang, Y. Xu, J. Zeng, H. Wang, H. Liu, Y. Zhao, S. Shi, M. Shakouri, H. Liang, Z. Wang, H. Zhang, Y. Hu, Z. Yao, D. Sinton and J. Li, *Nature Synthesis*, 2025, DOI: 10.1038/s44160-025-00868-7.
5. J. Li, R. Cai, H. Mu, J. Guo, X. Zhong, J. Wang, X. Du, J. Zhang and F. Li, *ACS Catalysis*, 2024, 14, 3266-3277.
6. S. Wang, F. Li, J. Zhao, Y. Zeng, Y. Li, Z.-Y. Lin, T.-J. Lee, S. Liu, X. Ren, W. Wang, Y. Chen, S.-F. Hung, Y.-R. Lu, Y. Cui, X. Yang, X. Li, Y. Huang and B. Liu, *Nature Communications*, 2024, 15, 10247.
7. J. Zhou, B. He, P. Huang, D. Wang, Z. Zhuang, J. Xu, C. Pan, Y. Dong, D. Wang, Y. Wang, H. Huang, J. Zhang and Y. Zhu, *Angewandte Chemie International Edition*, 2025, 64, e202418459.
8. T. Zhang, B. Yuan, W. Wang, J. He and X. Xiang, *Angewandte Chemie International Edition*, 2023, 62, e202302096.
9. P. Huang, Z. Yang, K. Zhai, B. Huang, J. Zhou, X. Sun, Y. Lin, J. Xu, C. Pan, Y. Dong, Y. Wang, Y. Zhang, Y. Lou, H. Huang, Y. Zhu and J. Zhang, *Journal of the American Chemical Society*, 2025, 147, 22062-22071.